Disordered ground state in the spin-orbit coupled Jeff = 1/2 distorted honeycomb magnet BiYbGeO5

S. Mohanty, S. S. Islam, N. Winterhalter-Stocker, Anton Jesche, G. Simutis, Ch. Wang, Z. Guguchia, J. Sichelschmidt, M. Baenitz, Alexander A. Tsirlin, Philipp Gegenwart, R. Nath

Angaben zur Veröffentlichung / Publication details:

Mohanty, S., S. S. Islam, N. Winterhalter-Stocker, Anton Jesche, G. Simutis, Ch. Wang, Z. Guguchia, et al. 2023. "Disordered ground state in the spin-orbit coupled Jeff = 1/2 distorted honeycomb magnet BiYbGeO5." *Physical Review B* 108 (13): 134408. https://doi.org/10.1103/physrevb.108.134408.

Disordered ground state in the spin-orbit coupled $J_{\text{eff}} = \frac{1}{2}$ distorted honeycomb magnet $BiYbGeO_5$

S. Mohanty,[1] S. S. Islam,[1] N. Winterhalter-Stocker,[2] A. Jesche,[2] G. Simutis,[3] Ch. Wang,[4] Z. Guguchia,[4] J. Sichelschmidt,[5] M. Baenitz,[5] A. A. Tsirlin,[6] P. Gegenwart,[2] and R. Nath[1,*]

[1]*School of Physics, Indian Institute of Science Education and Research, Thiruvananthapuram 695551, India*
[2]*Center for Electronic Correlations and Magnetism, University of Augsburg, 86159 Augsburg, Germany*
[3]*Laboratory for Neutron and Muon Instrumentation, Paul Scherrer Institut, 5232 Villigen PSI, Switzerland*
[4]*Laboratory for Muon Spin Spectroscopy, Paul Scherrer Institut, 5232 Villigen PSI, Switzerland*
[5]*Max Planck Institute for Chemical Physics of Solids, Nothnitzer Strasse 40, 01187 Dresden, Germany*
[6]*Felix Bloch Institute for Solid-State Physics, Leipzig University, 04103 Leipzig, Germany*

(Received 17 May 2023; revised 21 September 2023; accepted 22 September 2023; published 9 October 2023)

We delineate quantum magnetism in the strongly spin-orbit coupled distorted honeycomb lattice antiferromagnet $BiYbGeO_5$. Our magnetization and heat capacity measurements reveal that its low-temperature behavior is well described by an effective $J_{\text{eff}} = \frac{1}{2}$ Kramers doublet of Yb^{3+}. The ground state is nonmagnetic with a tiny spin gap. Temperature-dependent magnetic susceptibility, magnetization isotherm, and heat capacity can be modeled well assuming isolated spin dimers with anisotropic exchange interactions $J_Z \simeq 2.6$ K and $J_{XY} \simeq 1.3$ K. Heat capacity measurements backed by muon spin relaxation suggest the absence of magnetic long-range order down to at least 80 mK both in zero field and in applied fields. This sets $BiYbGeO_5$ apart from $Yb_2Si_2O_7$, with its unusual regime of magnon Bose-Einstein condensation, and suggests negligible interdimer couplings, despite only a weak structural deformation of the honeycomb lattice.

DOI: 10.1103/PhysRevB.108.134408

I. INTRODUCTION

The antiferromagnetic spin-$\frac{1}{2}$ dimer is the simplest case of a quantum magnet characterized by the singlet ($S = 0$) ground state with entangled spins and an excitation gap in the energy spectrum. Closing this gap by applying external magnetic fields has been instrumental in stabilizing long-range order in spin-dimer systems [1]. For the SU(2) symmetry of the underlying spin Hamiltonian, such order is often described in terms of Bose-Einstein condensation of magnons [2,3]. Experimental manifestations of this scenario include field-induced ordered states of $3d$ magnets with spin-dimer geometry [1,3–6]. More recently, similar effects were observed in the $4f$ magnet $Yb_2Si_2O_7$, although two distinct ordered states were reported in this case [7]. Different microscopic mechanisms were proposed for this behavior, including the weak, hitherto not detected anisotropy of Yb^{3+} [8] and the special geometry of interdimer interactions that arises from the underlying honeycomb lattice [9].

The magnetism of Yb^{3+} ions is often anisotropic. The anisotropic nature of the ion itself, as well as exchange anisotropy of magnetic couplings, may be behind many interesting effects, including the possible realization of quantum spin ice in pyrochlore materials [10–12], persistent dynamics observed in triangular spin-liquid candidates [13,14], and Tomonaga-Luttinger liquid behavior with spinon confinement-deconfinement transitions in spin-chain magnets [15]. Yb-based honeycomb magnets are currently studied as potential hosts for Kitaev physics [16–19]. Concurrently, deformed honeycomb lattices of Yb^{3+} could provide an interesting link to $Yb_2Si_2O_7$ and reveal the effect of magnetic anisotropy on the field-induced states of a dimer magnet.

Herein, we report one such case, the quantum magnet $BiYbGeO_5$ [20], which features a quasi-two-dimensional distorted honeycomb lattice of Yb^{3+} ions in the ac plane of the structure (see Fig. 1). This geometry is very similar to the one known from $Yb_2Si_2O_7$ [7]. In the $BiYbGeO_5$ case, the two-dimensional honeycomb layers are strongly buckled and, consequently, deformed. On the other hand, the two nearest-neighbor Yb^{3+}-Yb^{3+} distances remain similar, $d_1 = 3.492$ Å (dimer bond J_0) and $d_2 = 3.590$ Å (interdimer bonds J'). We elucidate the low-energy states of Yb^{3+} as a Kramers doublet described by an effective spin $J_{\text{eff}} = \frac{1}{2}$, establish the dimerized regime ($J_0 \gg J'$) with a disordered ground state, and examine the possibility of a field-induced magnetic order in this material.

II. METHODS

Polycrystalline samples of isostructural $BiRGeO_5$ (R = Yb, Y) were synthesized via the conventional solid-state synthesis technique. Bi_2O_3 (99.99%, Sigma Aldrich), GeO_2 (99.99%, Sigma Aldrich), and R_2O_3 (99.99%, Sigma Aldrich) were used as precursors. The stoichiometric mixtures of the starting materials were thoroughly ground, pressed into pellets, heated in a platinum crucible at 950 °C for 2 days in air, and then quenched. A 4% excess of Bi_2O_3 was used to get the pure phase of $BiRGeO_5$. In order to confirm the phase purity and crystal structure of the samples, powder x-ray diffraction

*rnath@iisertvm.ac.in

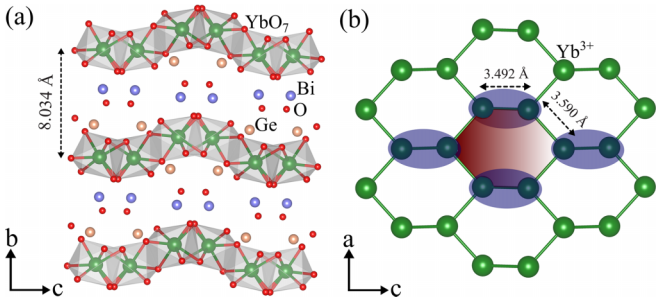

FIG. 1. (a) Crystal structure of $BiYbGeO_5$ viewed along the *a* axis, showing well-separated honeycomb layers formed by edge-shared YbO_7 polyhedra. (b) A section of the honeycomb layer projected onto the *ac* plane highlights the short Yb^{3+}-Yb^{3+} distance that leads to spin dimerization.

(XRD) measurement was performed at room temperature using the PANalytical x-ray diffractometer (Cu $K\alpha$ radiation, $\lambda_{av} \simeq 1.5418$ Å). Rietveld refinement of the XRD data was carried out using the FULLPROF software package [21], which confirms the formation of pure phase shown in Fig. 2. All peaks in the XRD data could be appropriately indexed by the orthorhombic space group *Pbca* (No. 61), and the obtained lattice parameters at room temperature are $a = 5.2948(1)$ Å,

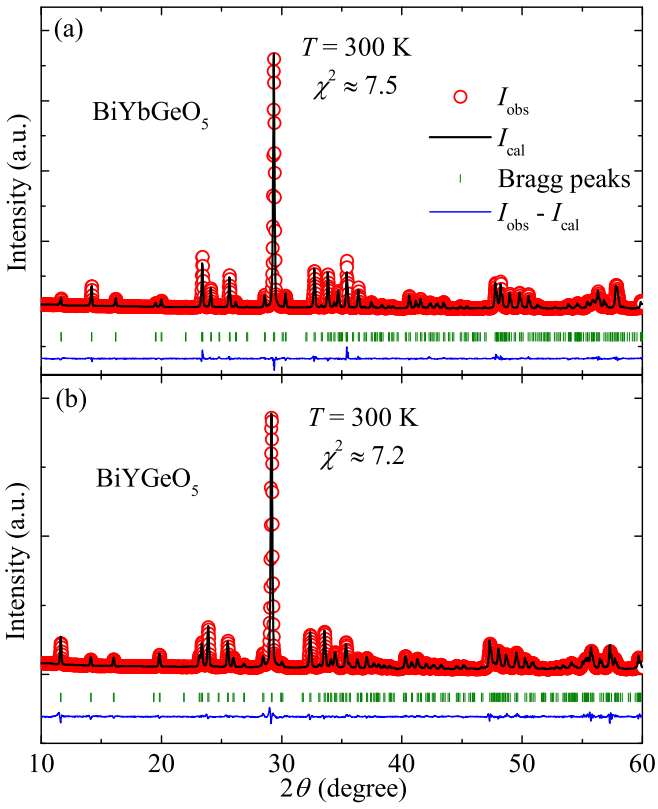

FIG. 2. Powder XRD pattern (open circles) at $T = 300$ K for (a) $BiYbGeO_5$ and (b) $BiYGeO_5$. The black solid line represents the Rietveld fit of the data. Expected Bragg peak positions are indicated by green vertical bars, and the solid blue line at the bottom denotes the difference between experimental and calculated intensities. The goodness of fit is $\chi^2 \simeq 7.5$ and 7.2, respectively.

TABLE I. The Wyckoff positions and the refined atomic coordinates (*x*, *y*, and *z*) for each atom at room temperature for $Bi(Yb,Y)GeO_5$.

Atom	Site	*x*	*y*	*z*	Occupancy
Bi1	8c	0.9560(3)	0.2382(1)	0.1458(1)	1
		0.9552(3)	0.2383(3)	0.1470(3)	1
Yb1	8c	0.0119(5)	0.0514(1)	0.3600(2)	1
Y1		0.0043(2)	0.0528(3)	0.3611(3)	1
Ge1	8c	0.0085(1)	0.4035(2)	0.4021(3)	1
		0.0098(2)	0.4055(3)	0.4055(3)	1
O1	8c	0.0385(4)	0.2755(1)	0.3534(1)	1
		0.0660(2)	0.3193(2)	0.3398(2)	1
O2	8c	0.3034(4)	0.4278(1)	0.4333(2)	1
		0.3203(2)	0.4402(2)	0.4496(2)	1
O3	8c	0.3154(3)	0.0922(2)	0.4743(1)	1
		0.2991(2)	0.1085(2)	0.4920(2)	1
O4	8c	0.2574(6)	0.1718(1)	0.2605(4)	1
		0.2702(2)	0.1447(2)	0.2442(2)	1
O5	8c	0.3408(3)	0.4699(1)	0.1998(1)	1
		0.3599(2)	0.4797(2)	0.1969(2)	1

$b = 15.2015(2)$ Å, $c = 10.9437(2)$ Å, and $V_{cell} \simeq 880.85(3)$, which are fairly comparable to those in a previous report [20]. The atomic coordinates of different atoms after the refinement are tabulated in Table I.

Magnetization *M* was measured with the help of a superconducting quantum interference device magnetometer (MPMS-3, Quantum Design) down to 0.4 K using an additional ^{3}He (iHelium3, Quantum Design, Japan) attachment. Heat capacity $C_p(T)$ for $T > 1.8$ K was measured on a small piece of sintered pellet using the relaxation technique in the physical property measurement system (Quantum Design). For the measurements in the millikelvin range, we used a pellet of the mixture (1:1 ratio) of $BiYbGeO_5$ and fine Ag powder with a total mass of 9.41 mg, and the measurements were carried out using the thermal relaxation method with a home-built setup installed in a dilution refrigerator. Here, the fine Ag powder is crucial for realizing good thermal contact at low temperatures. The contribution of the Ag powder to the heat capacity was determined from a polynomic function with the coefficients from Ref. [22] and subtracted from total measured heat capacity.

Muon spin relaxation (μSR) measurements were carried out on the powder sample at the Swiss Muon Source (SμS), Paul Scherrer Institute, Switzerland, using a combination of two spectrometers down to below 100 mK. The high-temperature measurements (1.5–50 K) were performed using a low-background, high-throughput instrument, the General Purpose Spectrometer (GPS), in zero field as well as in longitudinal fields [23]. The low-temperature measurements in both zero and transverse fields were performed using the standard settings of the high-field and low-temperature instrument (HAL) spectrometer, which allowed reaching temperatures as low as 12 mK. For measurement purposes, the powder sample was packed in silver foil envelopes, attached to a silver plate, and mounted on the cold finger of the dilution refrigerator. Ag was used because of its small nuclear magnetic moment,

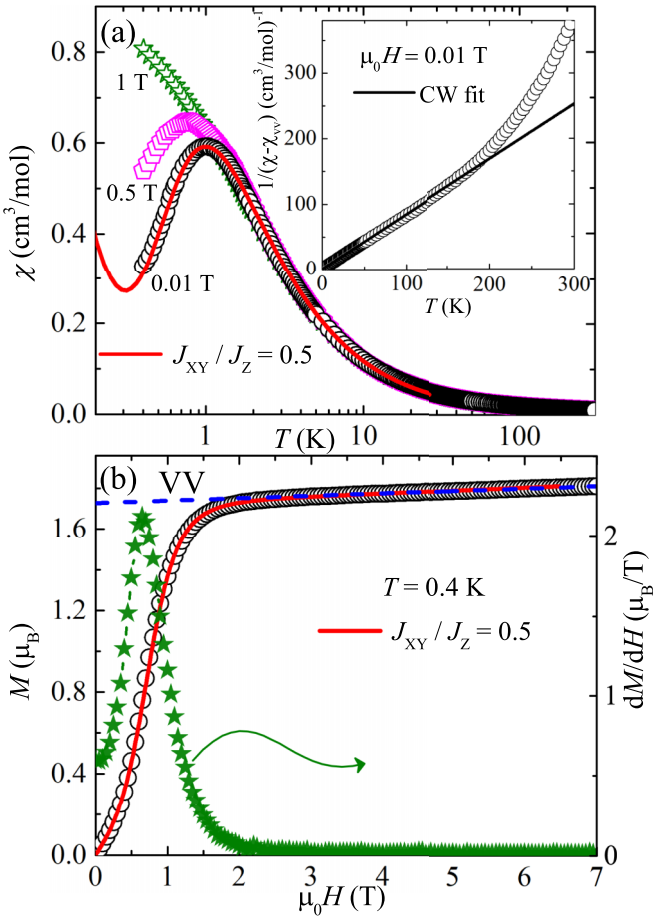

FIG. 3. (a) $\chi(T)$ of $BiYbGeO_5$ measured in different fields. The solid line represents the simulation for isolated spin dimers with anisotropic interactions ($J_z = 2.6$ K and $J_{xy} = 1.3$ K) for $\mu_0H = 0.01$ T. Inset: CW fit to the low-T $1/\chi$ data (after subtracting the Van Vleck contribution). (b) M vs H and dM/dH vs H in the left and right y axes, respectively, measured at $T = 0.4$ K. The horizontal dashed line marks the Van Vleck contribution. The solid line shows the simulation.

which minimizes the background depolarization of the muon spin ensemble.

The magnetization and heat capacity of the anisotropic spin dimer were obtained by exact diagonalization using the FULLDIAG utility of the ALPS package [24], where the number of sites is taken to be $Z = 2$.

III. RESULTS

A. Magnetization

Magnetic susceptibility χ as a function of T in different applied fields is depicted in Fig. 3(a). For $\mu_0H \simeq 0.01$ T, $\chi(T)$ increases with decreasing T in a Curie-Weiss (CW) manner and portrays a broad maximum centered at around 1 K, followed by a rapid decrease. No clear signature of magnetic long-range order (LRO) is evident down to 0.4 K. A weak upturn at very low temperatures is likely due to the presence of a small extrinsic paramagnetic contribution and/or defects [25]. With increasing field, the broad maximum is suppressed towards low temperatures. This broad maximum reflects the short-range correlations anticipated for a low-dimensional antiferromagnetic (AFM) spin system, and the rapid decrease signals the opening of a spin gap at low temperatures [26–28].

Above 150 K, the inverse susceptibility $1/\chi$ for $\mu_0H = 0.01$ T was fitted well by $\chi(T) = \chi_0 + \frac{C}{T-\theta_{CW}}$, where χ_0 is the temperature-independent susceptibility and the second term is the CW law. The fit yields $\chi_0 = 1.51(6) \times 10^{-3}$ cm^3/mol, the high-T effective moment μ_{eff}^{HT} ($= \sqrt{3k_BC/N_A}$, where C, k_B, and N_A are the Curie constant, Boltzmann's constant, and Avogadro's number, respectively) $= 4.78(3)\mu_B$, and the high-T CW temperature $\theta_{CW}^{HT} = -67(1)$ K (see the Supplemental Material (SM) [29]). This value of μ_{eff}^{HT} is in good agreement with the expected value, $\mu_{eff} = g\sqrt{J(J+1)} \simeq 4.54\mu_B$ for Yb^{3+} ($J = 7/2, g = 8/7$) in the $^4f_{13}$ configuration.

Inverse susceptibility $1/\chi$ is found to deviate from linearity at low temperatures with a clear slope change. After subtraction of the Van Vleck susceptibility χ_{VV}, obtained from the M vs H analysis, $1/(\chi - \chi_{VV})$ shows a linear regime at low temperatures [see the inset of Fig. 3(a)]. A CW fit in the T range of 10–30 K yields $\mu_{eff} = 3.07(1)\mu_B$ and $\theta_{CW} = -0.67(2)$ K. The negative value of θ_{CW} reflects the dominant AFM exchange between the Yb^{3+} ions. This experimental μ_{eff} corresponds to an effective spin $J_{eff} = \frac{1}{2}$ with an average $g = 3.5(2)$ [30]. Such a large value of g compared to the free-electron value of $g = 2.0$ reflects strong spin-orbit coupling and is consistent with the one obtained from the ESR experiments (see the SM [29]). In Yb^{3+}-based compounds, the Kramers doublets ($m_J = \pm 1/2$) evoked by the crystal electric field (CEF) excitations essentially control the magnetic properties at low temperatures. In such a scenario, the ground state is an effective $J_{eff} = \frac{1}{2}$ state, while the excited states generate a significant χ_{VV} [31–33]. Our $\chi(T)$ analysis supports the interpretation in terms of an effective pseudospin-1/2 ground state, similar to other Yb^{3+}-based compounds [31,34].

Figure 3(b) presents the magnetic isotherm (M vs H) measured at $T = 0.4$ K. It manifests a distinct curvature and then the tendency of saturation but increases very weakly with a further increase in field due to the Van Vleck contribution. The linear fit to the high-field ($\geqslant$6 T) data returns a slope of $\sim 0.012\mu_B$/T, which corresponds to $\chi_{VV} = 6.7(1) \times 10^{-3}$ cm^3/mol. From the y intercept of the linear fit, the saturation magnetization is estimated to be $M_S = 1.7(1)\mu_B$, which is in good agreement with $M_S = gJ_{eff}\mu_B \simeq 1.75\mu_B$, expected for $J_{eff} = \frac{1}{2}$ with powder-averaged $g \simeq 3.5$ [30]. Thus, the M vs H analysis also supports the $J_{eff} = \frac{1}{2}$ ground state of Yb^{3+}.

B. Heat capacity

Zero-field heat capacity [Fig. 4(a)] exhibits a broad maximum at $\sim$0.6 K and then decreases rapidly with temperature. While the broad maximum is attributed to the onset of short-range correlations, the rapid decrease is a hallmark of the formation of the singlet ground state [1,35]. A small upturn at very low temperatures (< 0.1 K) may be ascribed to the nuclear contribution to C_p [35]. When magnetic field is applied, initially, the broad maximum is strongly suppressed for $\mu_0H < 1$ T, suggesting the suppression of AFM correlations and the closing of spin gap [36]. For $\mu_0H > 1$ T, the position of the broad maximum shifts toward high temperatures, and its amplitude is enhanced significantly. Finally, for

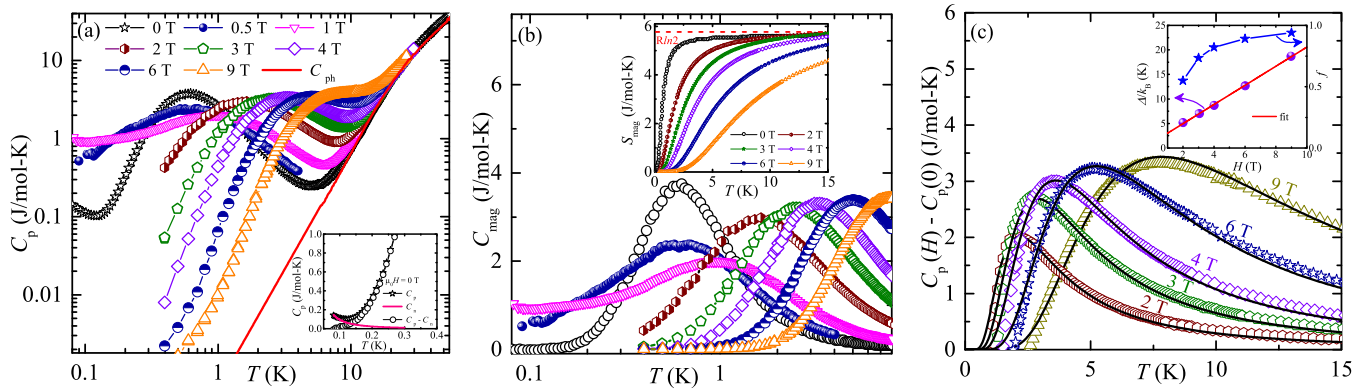

FIG. 4. (a) C_p vs T for $BiYbGeO_5$ measured in different applied fields. The solid line represents $C_{ph}(T)$ of the nonmagnetic analog $BiYGeO_5$. Inset: Zero-field C_p vs T in the low-temperature regime. The solid line represents the nuclear contribution C_n. (b) Magnetic heat capacity C_{mag} vs T in different magnetic fields. Inset: Magnetic entropy S_{mag} vs T in different magnetic fields. (c) Electronic Schottky contribution $[C_p(H) - C_p(0)]$ vs T along with the fit using Eq. (1). Inset: Δ/k_B and f vs H in the left and right y axes, respectively. The solid line represents the straight line fit to Δ/k_B vs H.

$\mu_0 H > 2$ T the height of the maximum almost saturates in the fully polarized state. This magnetic-field-driven broad maximum is a clear evidence of the Schottky anomaly due to the Zeeman splitting of the ground-state Kramers doublet.

The heat capacity of the nonmagnetic analog $BiYGeO_5$, which represents the phononic contribution C_{ph}, was measured down to 2 K and extrapolated to 80 mK by a T^3 fit to the low-temperature data. The magnetic heat capacity C_{mag} obtained by subtracting C_{ph} from the measured C_p in different fields is shown in Fig. 4(b). In zero field, the nuclear contribution is removed by fitting the data below 0.12 K by $C_n(T) = \alpha_Q/T^2$ [see the inset of Fig. 4(a)]. The fit yields the coefficient $\alpha_Q = 9.1(2) \times 10^{-4}$ J K/mol, which is in reasonable agreement with that reported for other Yb-based systems [37]. The obtained $C_{mag}(T)$ is then used to estimate the magnetic entropy $S_{mag}(T)$ by integrating $C_{mag}(T)/T$ in the measured T range [inset of Fig. 4(b)]. $S_{mag}(T)$ reaches a well-defined plateau at $R \ln 2$ in zero field, further endorsing the fact that the low-temperature properties can be explained by the $J_{eff} = \frac{1}{2}$ state [32,38,39]. In zero field, C_{mag} decays rapidly below the broad maximum, reflecting the singlet ground state.

To evaluate the Schottky contribution quantitatively, the zero-field data $C_p(T, H = 0)$ are subtracted from the high-field data $C_p(T, H)$ [i.e., $C_{Sch}(T, H) = C_p(T, H) - C_p(T, H = 0)$]. In Fig. 4(c), $C_{Sch}(T, H)$ is fitted by the two-level Schottky function [40]

$$C_{Sch}(T) = fR\left(\frac{\Delta}{k_B T}\right)^2 \frac{e^{(\Delta/k_B T)}}{[1 + e^{(\Delta/k_B T)}]^2}, \qquad (1)$$

where f is the fraction of free spins excited by the applied field, Δ/k_B is the crystal-field gap between the ground state and the first excited Kramers doublet, and R is the gas constant. The inset of Fig. 4(c) presents the obtained f and Δ/k_B as a function of H on the right and left y axes, respectively. f increases with H and then reaches a constant value of about $\sim$1 for $\mu_0 H > 3$ T, confirming that magnetic field splits the energy levels and excites the free Yb^{3+} spins to the higher-energy levels and nearly 100% of spins are excited above the saturation field. Similarly, the maximum of the $C_p(H)$-$C_p(0)$ curves almost reaches a constant value for $\mu_0 H > 3$ T, suggesting that $\sim$100% spins become free in higher fields. Further, Δ/k_B increases linearly with H, and a straight line fit returns the zero-field energy gap $\Delta/k_B(0) \simeq 1.07(4)$ K, which possibly indicates an intrinsic field in the system [41]. Using the value of $\Delta/k_B \simeq 18.8$ K at 9 T in $\Delta/k_B = g\mu_B H/k_B$, the g value is estimated to be $g \simeq 3.5$, which is consistent with the magnetization analysis.

C. Muon spin relaxation

Because of its much shorter time window (10 ns–15 μs), μSR is an excellent probe in tracing the dynamics of slowly fluctuating magnetic moments, especially low-dimensional magnets. The zero-field μ^+ spin depolarization rate λ is related to the spin-spin correlation function as $\lambda = \gamma_\mu^2 \int_0^\infty \langle B_{loc}^\perp(t) B_{loc}^\perp(0)\rangle\, dt \propto S_{\omega\to 0}^\perp$, where $S_{\omega\to 0}^\perp = \int_0^\infty \langle s_i^\perp(t) s_i^\perp(0)\rangle\, dt$ is the static spin structure factor [42,43]. Thus, by measuring muon asymmetry as a function of temperature one can understand the correlated behavior of a spin system.

The muon asymmetry curves measured at different temperatures in zero field are displayed in Fig. 5. The absence of oscillations as well as a nonoscillating undamped 1/3 tail in the muon spin polarization down to 12 mK corroborate the absence of a magnetic LRO. The asymmetry curves follow a stretched exponential behavior $A(t) = A(0)\, e^{-(\lambda t)^\beta}$ with only a small temperature dependence, a footprint of the dynamics of a disordered (singlet) state [44]. The stretched-exponential behavior suggests that there is a distribution of relaxation rates [30,43]. The value of β is found to be constant and less than 1 ($\sim$0.73) over the entire temperature range, which indicates a distribution possibly due to weak disorder at the O site (muon stopping site). The estimated depolarization rate λ as a function of T is presented in the inset of Fig. 5. It is almost constant at high temperatures, exhibits a drop below $\sim$4 K, and reaches a constant value below around 1 K. This behavior is reproduced well by an activated function, $\lambda \propto e^{-(\Delta_\mu/k_B T)}$ with a spin gap of $\Delta_\mu/k_B = 1.7(2)$ K, further endorsing a singlet ground state with no magnetic LRO [45].

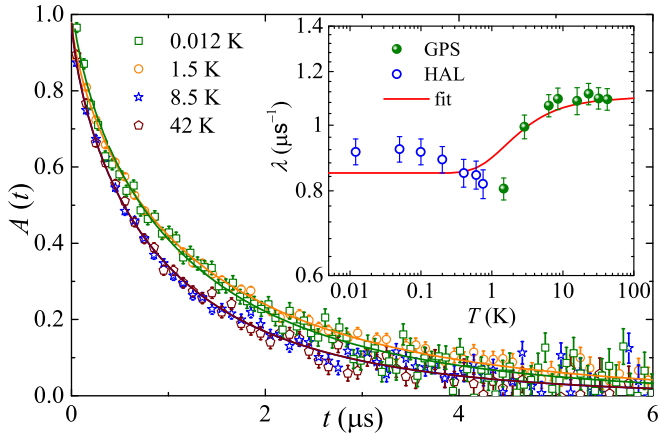

FIG. 5. Muon decay asymmetry vs time in zero field at four different temperatures, with solid lines being the exponential fits. Inset: λ vs T from both the GPS and HAL spectrometers together with the fit using an activated behavior (solid line) with $\Delta_\mu/k_B \simeq 1.7$ K.

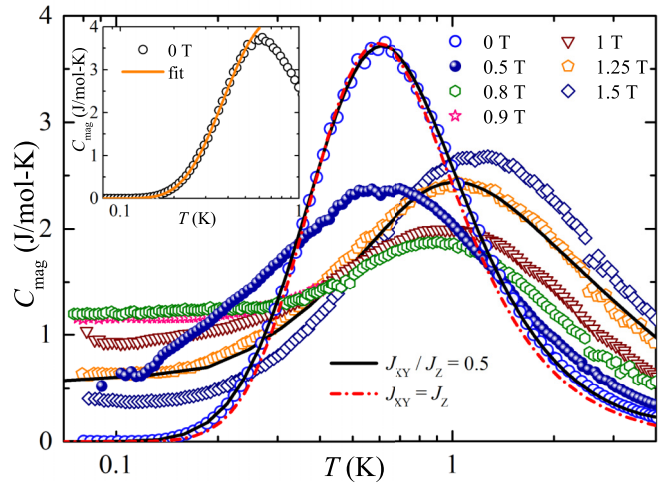

FIG. 6. Magnetic heat capacity C_{mag} vs T, measured down to 0.08 K in different fields. The solid and dashed lines represent simulated curves for an isolated spin-$\frac{1}{2}$ dimer with either isotropic or anisotropic exchange interactions. We also show the simulation for the anisotropic spin-$\frac{1}{2}$ dimer in an applied field of 1.25 T where powder averaging was taken into account. Inset: Zero-field C_{mag} vs T; the solid line is an exponential fit with $\Delta/k_B = 1.5(1)$ K.

IV. DISCUSSION

Deformation of the honeycomb spin lattice in $BiYbGeO_5$ potentially allows different microscopic regimes: (i) weakly distorted honeycombs ($J_0 \simeq J'$), (ii) spin dimers ($J_0 \gg J'$), and (iii) spin chains ($J' \gg J_0$). The first scenario should lead to a magnetic LRO already in zero field, as previously observed in $YbCl_3$ with its weakly distorted honeycombs [16,17]. The absence of LRO in zero field excludes this scenario. Assuming Heisenberg interactions, the spin dimer can be distinguished from the spin chain by the presence and absence of a spin gap, respectively. The gapped state observed experimentally in $BiYbGeO_5$ favors the dimer scenario.

Direct simulation of the magnetic heat capacity for the Heisenberg spin dimer shows reasonable agreement with the experiment (Fig. 6). However, close inspection of the data reveals that the maximum of the simulated curve is narrower than the experimental one. This discrepancy can be remedied by considering an anisotropic exchange coupling,

$$\mathcal{H} = J_{XY}\left(S_i^x S_j^x + S_i^y S_j^y\right) + J_Z S_i^z S_j^z, \qquad (2)$$

with $J_{XY} \simeq 1.3$ K and $J_Z \simeq 2.6$ K. The anisotropy $J_{XY}/J_Z \simeq 0.5$ controls the width of the maximum and can be determined rather accurately even with powder data. $\chi(T)$ and M vs H curves are well reproduced with the same parameters assuming isotropic $g = 3.5$ (see Fig. 3). The Van Vleck term, $\chi_{VV} = 0.012\ \mu_B$/T, was added in the case of $M(H)$, whereas the $\chi(T)$ fit included an impurity contribution $C_{imp}/(T - \theta_{imp})$, with $C_{imp} = 0.05$ cm^3 K/mol and $\theta_{imp} = 0.07$ K. This value of C_{imp} corresponds to an impurity spin concentration of nearly ~4.2%, assuming the impurity spins $S = 1/2$ and $g = 3.5$.

Further, the spin gap extracted by fitting the zero-field $C_{mag}(T)$ below 0.4 K with an exponential function, $C_{mag} \propto (\frac{\Delta}{k_B T})^2 e^{-\Delta/k_B T}$, which is the low-$T$ approximation of the spin-$\frac{1}{2}$ dimer model [35], returns the value of $\Delta/k_B = 1.5(1)$ K (see the inset of Fig. 6). This value matches well with the average intradimer coupling $J_0 = \frac{2J_{XY}+J_Z}{3} \simeq 1.72$ K, as well as the gap value obtained from the μSR analysis.

The excellent fit of thermodynamic data with the model of isolated spin dimers, Eq. (2), suggests that any interdimer couplings are likely negligible ($\leqslant$60 mK). The weakness of these couplings is in line with the fact that signatures of magnetic LRO have been observed neither in zero field nor in applied fields down to at least 80 mK. We thus conclude that $BiYbGeO_5$ is well described by the model of isolated anisotropic spin dimers, similar to $NaLu_{0.9}Yb_{0.1}Se_2$ [46]. This result may look unexpected considering a rather weak geometrical distortion of the honeycomb layer, $2(d_1 - d_2)/(d_1 + d_2) = 2.8\%$, which is comparable to 3.4% in $Yb_2Si_2O_7$ [7]. However, the honeycomb layers in $BiYbGeO_5$ are strongly buckled, unlike in the silicate. According to Fig. 1, the dimer coupling J_0 occurs in the flat part of the layer, whereas the interdimer bonds J' lie on the folding line and may be strongly affected by the buckling. Moreover, the coordination of Yb^{3+} changes from sixfold in $Yb_2Si_2O_7$ to sevenfold in $BiYbGeO_5$. This may change the nature of the ground-state Kramers doublet and lead to a significant modification of the exchange couplings.

V. CONCLUSION

$BiYbGeO_5$ features a distorted honeycomb arrangement of the $J_{eff} = 1/2$ Yb^{3+} ions. We showed that magnetism of this material is well described by the model of anisotropic spin dimers. The quantum disordered state with a spin gap was observed in zero magnetic field, and no LRO reminiscent of Bose-Einstein condensation of triplons was induced by the applied field down to at least 80 mK, in contrast to typical spin-dimer magnets. We ascribe this behavior to the fact that spin dimers are magnetically nearly isolated. This sets $BiYbGeO_5$ apart from another Yb-based dimer magnet, $Yb_2Si_2O_7$, which shows a similar deformation of the honeycomb lattice but lacks the buckling of the structural layers.

Additional data associated with this manuscript can be found in Ref. [47].

ACKNOWLEDGMENTS

We would like to acknowledge SERB, India, for financial support bearing Sanction Grant No. CRG/2022/000997. Part of this work is based on experiments performed at the Swiss Muon Source SμS, Paul Scherrer Institute, Villigen, Switzerland. The project received funding from the European Union's Horizon 2020 research and innovation program under Marie Skłodowska-Curie Grant Agreement No. 884104 (PSI-FELLOW-III-3i). Computations for this work were done using resources of the Leipzig University Computing Center. This work was supported by the German Research Foundation (DFG) via Project No. 492547816 (TRR360).

[1] V. Zapf, M. Jaime, and C. D. Batista, Bose-Einstein condensation in quantum magnets, Rev. Mod. Phys. **86**, 563 (2014).

[2] T. M. Rice, To condense or not to condense, Science **298**, 760 (2002).

[3] T. Giamarchi, C. Rüegg, and O. Tchernyshyov, Bose-Einstein condensation in magnetic insulators, Nat. Phys. **4**, 198 (2008).

[4] T. Nikuni, M. Oshikawa, A. Oosawa, and H. Tanaka, Bose-Einstein condensation of dilute magnons in $TlCuCl_3$, Phys. Rev. Lett. **84**, 5868 (2000).

[5] M. Jaime, V. F. Correa, N. Harrison, C. D. Batista, N. Kawashima, Y. Kazuma, G. A. Jorge, R. Stern, I. Heinmaa, S. A. Zvyagin, Y. Sasago, and K. Uchinokura, Magnetic-field-induced condensation of triplons in Han Purple pigment $BaCuSi_2O_6$, Phys. Rev. Lett. **93**, 087203 (2004).

[6] P. K. Mukharjee, K. M. Ranjith, B. Koo, J. Sichelschmidt, M. Baenitz, Y. Skourski, Y. Inagaki, Y. Furukawa, A. A. Tsirlin, and R. Nath, Bose-Einstein condensation of triplons close to the quantum critical point in the quasi-one-dimensional spin-$\frac{1}{2}$ antiferromagnet $NaVOPO_4$, Phys. Rev. B **100**, 144433 (2019).

[7] G. Hester, H. S. Nair, T. Reeder, D. R. Yahne, T. N. DeLazzer, L. Berges, D. Ziat, J. R. Neilson, A. A. Aczel, G. Sala, J. A. Quilliam, and K. A. Ross, Novel strongly spin-orbit coupled quantum dimer magnet: $Yb_2Si_2O_7$, Phys. Rev. Lett. **123**, 027201 (2019).

[8] M. O. Flynn, T. E. Baker, S. Jindal, and R. R. P. Singh, Two phases inside the Bose condensation dome of $Yb_2Si_2O_7$, Phys. Rev. Lett. **126**, 067201 (2021).

[9] C. Feng, E. M. Stoudenmire, and A. Wietek, Bose-Einstein condensation in honeycomb dimer magnets and $Yb_2Si_2O_7$, Phys. Rev. B **107**, 205150 (2023).

[10] K. A. Ross, L. Savary, B. D. Gaulin, and L. Balents, Quantum excitations in quantum spin ice, Phys. Rev. X **1**, 021002 (2011).

[11] J. D. Thompson, P. A. McClarty, H. M. Rønnow, L. P. Regnault, A. Sorge, and M. J. P. Gingras, Rods of neutron scattering intensity in $Yb_2Ti_2O_7$: Compelling evidence for significant anisotropic exchange in a magnetic pyrochlore oxide, Phys. Rev. Lett. **106**, 187202 (2011).

[12] J. D. Thompson, P. A. McClarty, D. Prabhakaran, I. Cabrera, T. Guidi, and R. Coldea, Quasiparticle breakdown and spin Hamiltonian of the frustrated quantum pyrochlore $Yb_2Ti_2O_7$ in a magnetic field, Phys. Rev. Lett. **119**, 057203 (2017).

[13] Y. Li, P. Gegenwart, and A. A. Tsirlin, Spin liquids in geometrically perfect triangular antiferromagnets, J. Phys.: Condens. Matter **32**, 224004 (2020).

[14] J. A. M. Paddison, M. Daum, Z. Dun, G. Ehlers, Y. Liu, M. B. Stone, H. Zhou, and M. Mourigal, Continuous excitations of the triangular-lattice quantum spin liquid $YbMgGaO_4$, Nat. Phys. **13**, 117 (2017).

[15] L. S. Wu, S. E. Nikitin, Z. Wang, W. Zhu, C. D. Batista, A. M. Tsvelik, A. M. Samarakoon, D. A. Tennant, M. Brando, L. Vasylechko, M. Frontzek, A. T. Savici, G. Sala, G. Ehlers, A. D. Christianson, M. D. Lumsden, and A. Podlesnyak, Tomonaga-Luttinger liquid behavior and spinon confinement in $YbAlO_3$, Nat. Commun. **10**, 698 (2019).

[16] J. Xing, E. Feng, Y. Liu, E. Emmanouilidou, C. Hu, J. Liu, D. Graf, A. P. Ramirez, G. Chen, H. Cao, and N. Ni, Néel-type antiferromagnetic order and magnetic field–temperature phase diagram in the spin-$\frac{1}{2}$ rare-earth honeycomb compound $YbCl_3$, Phys. Rev. B **102**, 014427 (2020).

[17] G. Sala, M. B. Stone, B. K. Rai, A. F. May, P. Laurell, V. O. Garlea, N. P. Butch, M. D. Lumsden, G. Ehlers, G. Pokharel, A. Podlesnyak, D. Mandrus, D. S. Parker, S. Okamoto, G. B. Halász, and A. D. Christianson, Van Hove singularity in the magnon spectrum of the antiferromagnetic quantum honeycomb lattice, Nat. Commun. **12**, 171 (2021).

[18] Z. Zhang, Y. Cai, J. Kang, Z. Ouyang, Z. Zhang, A. Zhang, J. Ji, F. Jin, and Q. Zhang, Anisotropic exchange coupling and ground state phase diagram of Kitaev compound YbOCl, Phys. Rev. Res. **4**, 033006 (2022).

[19] C. Wessler, B. Roessli, K. W. Krämer, B. Delley, O. Waldmann, L. Keller, D. Cheptiakov, H. B. Braun, and M. Kenzelmann, Observation of plaquette fluctuations in the spin-1/2 honeycomb lattice, npj Quantum Mater. **5**, 85 (2020).

[20] C. Cascales, J. A. Campa, E. G. Puebla, M. A. Monge, C. R. Valero, and I. Rasines, New rare-earth (Y, Yb) bismuth(III) germanates. An initial study of a promising series, J. Mater. Chem. **12**, 3626 (2002).

[21] J. R. Carvajal, Recent advances in magnetic structure determination by neutron powder diffraction, Phys. B (Amsterdam, Neth.) **192**, 55 (1993).

[22] D. L. Martin, Specific heat of copper, silver, and gold below 30 °K, Phys. Rev. B **8**, 5357 (1973).

[23] A. Amato, H. Luetkens, K. Sedlak, A. Stoykov, R. Scheuermann, M. Elender, A. Raselli, and D. Graf, The new versatile general purpose surface-muon instrument (GPS) based on silicon photomultipliers for μSR measurements on a continuous-wave beam, Rev. Sci. Instrum. **88**, 093301 (2017).

[24] B. Bauer *et al.*, The ALPS project release 2.0: Open source software for strongly correlated systems, J. Stat. Mech. Theory Exp. (2011) P05001.

[25] A. A. Tsirlin, R. Nath, C. Geibel, and H. Rosner, Magnetic properties of $Ag_2VOP_2O_7$: An unexpected spin dimer system, Phys. Rev. B **77**, 104436 (2008).

[26] U. Arjun, K. M. Ranjith, B. Koo, J. Sichelschmidt, Y. Skourski, M. Baenitz, A. A. Tsirlin, and R. Nath, Singlet ground state in the alternating spin-$\frac{1}{2}$ chain compound $NaVOAsO_4$, Phys. Rev. B **99**, 014421 (2019).

[27] A. A. Tsirlin, R. Nath, J. Sichelschmidt, Y. Skourski, C. Geibel, and H. Rosner, Frustrated couplings between alternating spin-$\frac{1}{2}$ chains in $AgVOAsO_4$, Phys. Rev. B **83**, 144412 (2011).

[28] P. K. Mukharjee, K. M. Ranjith, M. Baenitz, Y. Skourski, A. A. Tsirlin, and R. Nath, Two types of alternating spin-$\frac{1}{2}$ chains and their field-induced transitions in ε-$LiVOPO_4$, Phys. Rev. B **101**, 224403 (2020).

[29] See Supplemental Material at http://link.aps.org/supplemental/10.1103/PhysRevB.108.134408 for further details on: Experimental details, Magnetization, Electron spin resonance, Muon spin relaxation, which includes Refs. [48–50].

[30] K. Somesh, S. S. Islam, S. Mohanty, G. Simutis, Z. Guguchia, C. Wang, J. Sichelschmidt, M. Baenitz, and R. Nath, Absence of magnetic order and emergence of unconventional fluctuations in the $J_{\text{eff}} = \frac{1}{2}$ triangular-lattice antiferromagnet $YbBO_3$, Phys. Rev. B **107**, 064421 (2023).

[31] Y. D. Li, X. Wang, and G. Chen, Anisotropic spin model of strong spin-orbit-coupled triangular antiferromagnets, Phys. Rev. B **94**, 035107 (2016).

[32] Y. Li, G. Chen, W. Tong, L. Pi, J. Liu, Z. Yang, X. Wang, and Q. Zhang, Rare-earth triangular lattice spin liquid: A single-crystal study of $YbMgGaO_4$, Phys. Rev. Lett. **115**, 167203 (2015).

[33] K. M. Ranjith, K. Brinda, U. Arjun, N. G. Hegde, and R. Nath, Double phase transition in the triangular antiferromagnet $Ba_3CoTa_2O_9$, J. Phys.: Condens. Matter **29**, 115804 (2017).

[34] R. Bag, M. Ennis, C. Liu, S. E. Dissanayake, Z. Shi, J. Liu, L. Balents, and S. Haravifard, Realization of quantum dipoles in triangular lattice crystal $Ba_3Yb(BO_3)_3$, Phys. Rev. B **104**, L220403 (2021); B. Schmidt, J. Sichelschmidt, K. M. Ranjith, T. Doert, and M. Baenitz, Yb delafossites: Unique exchange frustration of $4f$ spin-$\frac{1}{2}$ moments on a perfect triangular lattice, *ibid.* **103**, 214445 (2021).

[35] R. S. Freitas, W. A. Alves, and A. Paduan-Filho, Magnetic-field-induced ordered phase in the chloro-bridged copper(II) dimer system $[Cu_2(apyhist)_2Cl_2](ClO_4)_2$, Phys. Rev. B **95**, 184426 (2017).

[36] C. Rüegg, K. Kiefer, B. Thielemann, D. F. McMorrow, V. Zapf, B. Normand, M. B. Zvonarev, P. Bouillot, C. Kollath, T. Giamarchi, S. Capponi, D. Poilblanc, D. Biner, and K. W. Krämer, Thermodynamics of the spin Luttinger liquid in a model ladder material, Phys. Rev. Lett. **101**, 247202 (2008).

[37] K. M. Ranjith, S. Luther, T. Reimann, B. Schmidt, P. Schlender, J. Sichelschmidt, H. Yasuoka, A. M. Strydom, Y. Skourski, J. Wosnitza, H. Kühne, T. Doert, and M. Baenitz, Anisotropic field-induced ordering in the triangular-lattice quantum spin liquid $NaYbSe_2$, Phys. Rev. B **100**, 224417 (2019).

[38] S. Guo, A. Ghasemi, C. L. Broholm, and R. J. Cava, Magnetism on ideal triangular lattices in $NaBaYb(BO_3)_2$, Phys. Rev. Mater. **3**, 094404 (2019).

[39] Y. Tokiwa, S. Bachus, K. Kavita, A. Jesche, A. A. Tsirlin, and P. Gegenwart, Frustrated magnet for adiabatic demagnetization cooling to milli-kelvin temperatures, Commun. Mater. **2**, 42 (2021).

[40] C. Kittel, *Introduction to Solid State Physics* (Wiley, Hoboken, NJ, 2005).

[41] S. Kundu, A. Hossain, P. Keerthi, R. Das, M. Baenitz, P. J. Baker, J.-C. Orain, D. C. Joshi, R. Mathieu, P. Mahadevan, S. Pujari, S. Bhattacharjee, A. V. Mahajan, and D. D. Sarma, Signatures of a spin-$\frac{1}{2}$ cooperative paramagnet in the diluted triangular lattice of Y_2CuTiO_6, Phys. Rev. Lett. **125**, 117206 (2020).

[42] D. Bono, P. Mendels, G. Collin, N. Blanchard, F. Bert, A. Amato, C. Baines, and A. D. Hillier, μSR study of the quantum dynamics in the frustrated $S = \frac{3}{2}$ kagomé bilayers, Phys. Rev. Lett. **93**, 187201 (2004).

[43] Y. Li, D. Adroja, P. K. Biswas, P. J. Baker, Q. Zhang, J. Liu, A. A. Tsirlin, P. Gegenwart, and Q. Zhang, Muon spin relaxation evidence for the U(1) quantum spin-liquid ground state in the triangular antiferromagnet $YbMgGaO_4$, Phys. Rev. Lett. **117**, 097201 (2016).

[44] A. Yaouanc and P. D. de Réotier, *Muon Spin Rotation, Relaxation, and Resonance: Applications to Condensed Matter* (Oxford University Press, Oxford, 2011).

[45] R. C. Williams, W. J. A. Blackmore, S. P. M. Curley, M. R. Lees, S. M. Birnbaum, J. Singleton, B. M. Huddart, T. J. Hicken, T. Lancaster, S. J. Blundell, F. Xiao, A. Ozarowski, F. L. Pratt, D. J. Voneshen, Z. Guguchia, C. Baines, J. A. Schlueter, D. Y. Villa, J. L. Manson, and P. A. Goddard, Near-ideal molecule-based Haldane spin chain, Phys. Rev. Res. **2**, 013082 (2020).

[46] L. Pritchard Cairns, R. Day, S. Haley, N. Maksimovic, J. Rodriguez, H. Taghinejad, J. Singleton, and J. Analytis, Tracking the evolution from isolated dimers to many-body entanglement in $NaLu_xYb_{1-x}Se_2$, Phys. Rev. B **106**, 024404 (2022).

[47] https://doi.org/10.5281/zenodo.8406219.

[48] D. Rauch, M. Kraken, F. J. Litterst, S. Süllow, H. Luetkens, M. Brando, T. Förster, J. Sichelschmidt, A. Neubauer, C. Pfleiderer, W. J. Duncan, and F. M. Grosche, Spectroscopic study of metallic magnetism in single-crystalline $Nb_{1-y}Fe_{2+y}$, Phys. Rev. B **91**, 174404 (2015).

[49] A. A. Aczel, Y. Kohama, C. Marcenat, F. Weickert, M. Jaime, O. E. Ayala-Valenzuela, R. D. McDonald, S. D. Selesnic, H. A. Dabkowska, and G. M. Luke, Field-induced Bose-Einstein condensation of triplons up to 8 K in $Sr_3Cr_2O_8$, Phys. Rev. Lett. **103**, 207203 (2009).

[50] R. Orbach and B. Bleaney, Spin-lattice relaxation in rare-earth salts, Proc. Math. Phys. Eng. Sci. **264**, 458 (1961).